Double Stator Linear-Rotary Actuator with a Single Set of Mover Magnets

S. Miric,
M. Schuck,
A. Tüysüz,
J. W. Kolar

Double Stator Linear-Rotary Actuator with a Single Set of Mover Magnets

Spasoje Mirić, Marcel Schuck, Arda Tüysüz and Johann W. Kolar
Power Electronic Systems Laboratory, ETH Zürich, Switzerland
Email: miric@lem.ee.ethz.ch

Abstract—Double stator (DS) linear-rotary actuators (LiRAs) are mainly used in machining applications with high force and torque demands, such as milling or turning. The mover of a typical DS LiRA contains two sets of permanent magnets, one arranged as in radial-flux rotating machines and the other as in tubular linear machines. A back iron is sandwiched between these two sets of permanent magnets, rendering the mover heavy and bulky. Consequently, DS LiRAs are not suitable for applications with high dynamics, such as pick-and-place robots in the packaging and semiconductor industries. In order to increase the dynamics of DS LiRAs, two different ironless mover layouts are proposed in this work. The achievable forces and torques are calculated using finite element method (FEM) simulations and compared to the standard DS LiRA. Manufacturing limitations of the proposed mover layouts and their influence on the performance are considered. Moreover, cogging force and cogging torque of the standard and proposed LiRAs are compared. To verify the FEM models used in the analysis, a simplified test setup with a flat mover is presented. The flux linkage is measured and a good agreement with FEM simulations is demonstrated.

Index Terms—double-stator, high acceleration, linear-rotary actuator, permanent magnet actuator, pick-and-place

I. INTRODUCTION

Linear-rotary actuators (LiRAs) are used in many applications requiring coupled linear and rotary motion, such as gearbox control actuation in vehicles [1], tooling machines such as drills [2], robotics [3], and industrial pick-and-place machines [4], [5]. In order to achieve linear and rotary motion, linear and rotary actuators can be coupled in different ways. In usual LiRA arrangements, standalone linear and rotary actuators that share the same mover [5], [6] are displaced axially, as conceptually shown in Fig. 1. The mover consists
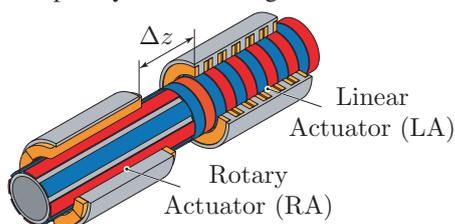
Fig. 1: LiRA with axially displaced stators.

of two axially displaced parts (linear and rotary) that produce force and torque by interacting with the respective part of the two stators. In order to keep the overlapping area and magnetic interaction between the mover and the stators constant, the latter are placed apart by an axial distance of Δz, which has to be larger than the axial stroke of the mover. Consequently, this results in an increased length of the LiRA.

Another approach is to stack the stators radially instead of axially [7], [8], i.e. by placing them on the inside and outside

of a hollow mover. Such a setup is commonly referred to as a double stator (DS) actuator and is shown in Fig. 2. In the displayed arrangement, the stator of the rotary actuator is located on the inside of the mover, while that of the linear actuator is placed outside. A detailed view of the conventional mover (CM) used is provided in Fig. 2(b). It consists of two sets of permanent magnets (PMs) and a back iron for magnetic decoupling of these sets of PMs. The PMs are arranged such that their north and south poles alternate in the axial and circumferential direction for the linear and rotary actuator, respectively. Naturally, an interchange of the actuators, i.e. a DS LiRA with an inner linear actuator and an outer rotary actuator, is also possible.
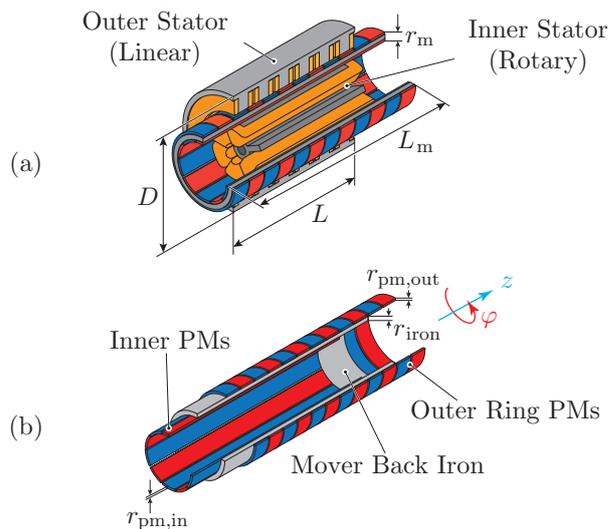
Fig. 2: (a) DS LiRA with inner rotary and outer linear actuators, where r_m denotes the mover thickness. (b) CM of the DS LiRA with two sets of PMs. The radial thickness of the mover is $r_\mathrm{m} = r_\mathrm{pm,in} + r_\mathrm{iron} + r_\mathrm{pm,out}$.

The advantage of the LiRA with radially stacked stators over that with axially displaced stators is its lower axial length. However, the requirement of a back iron results in a high mass and moment of inertia (MoM) of the CM. As a result, the dynamics (linear and circumferential accelerations) of the DS LiRA with CM are limited, which restricts its usage to applications with high force and torque demands rather than those requiring high dynamics.

The DS LiRA with CM designed in [7], which is similar to the one shown in Fig. 2, is used as an example in the following considerations. Based on the mass densities of the employed steel and rare earth PMs, an average mass density of the CM of $7 \times 10^3 \, \mathrm{kg \, m^{-3}}$ is assumed, resulting in an overall CM mass of $\approx 11.7 \, \mathrm{kg}$. Given the rated force of the actuator
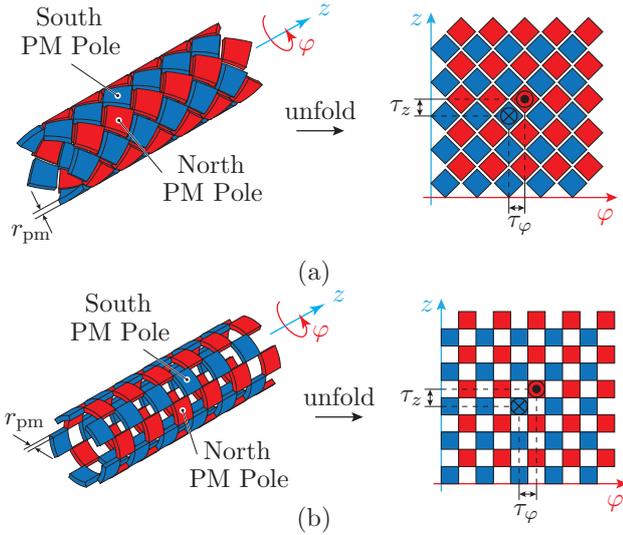
Fig. 3: Proposed ironless mover layouts for the DS LiRA with a single set of PMs. Mover layout with (a) diamond-shaped PMs referred to as DM, and (b) square-shaped PMs referred to as SM. The size of the axial and circumferential poles are denoted by τ_z and τ_φ, respectively. The mover thickness is equal to the PM thickness, $r_m = r_{pm}$.

TABLE I: Parameters of the simulated actuators shown in Fig. 4.

Parameter (Symbol)	Values		
PM remanent flux density	1.3 T		
Iron relative permeability	500		
	CM	**DM**	**SM**
Inner PM thickness ($r_{pm,in}$)	1 mm	-	-
Outer PM thickness ($r_{pm,out}$)	1 mm	-	-
Back iron thickness (r_{iron})	2 mm	-	-
PM thickness (r_{pm})	-	4 mm	4 mm
Mover thickness (r_m)	4 mm	4 mm	4 mm
Inner mover radius	11.5 mm	11.5 mm	11.5 mm
Outer mover radius	15.5 mm	15.5 mm	15.5 mm
Circumferential pole size (τ_φ)	36°	36°	36°
Axial pole size (τ_z)	7.5 mm	7.5 mm	7.5 mm

of $650\,\mathrm{N}$, the achievable axial acceleration is estimated to be $\approx 55\,\mathrm{m\,s^{-2}}$, where bearing friction has been neglected. This acceleration is about one third of that achieved by LiRAs used in applications requiring high dynamics. A LiRA which achieves a maximum linear acceleration of $150\,\mathrm{m\,s^{-2}}$ is presented in [4]. Aside from this, manufacturing of a DS LiRA with CM is challenging, as PMs have to be placed and fixed on both sides of the CM back iron.

In order to increase the dynamics and resolve the issues related to manufacturing of the DS with CM, two ironless mover layouts with a single set of PMs are proposed in this paper. A description and analysis of the new mover concept is provided in Sec. II and benchmarking against DS with the CM is carried out in Sec. III. Manufacturing limitations of the proposed mover layouts and their influence on the performance of the DS LiRA as well as the cogging torque and the cogging force are studied in Sec. IV. In Sec. V, a simplified hardware setup that was used to verify the employed FEM models is described. Section VI concludes the paper.

II. PROPOSED DOUBLE STATOR ACTUATOR

In this section, a DS LiRA with two different ironless mover layouts incorporating only a single set of PMs is proposed to overcome the drawbacks of the DS LiRA with CM (see Sec. I). The arrangement of PMs in the proposed mover is chosen such that north and south poles alternate in the axial and circumferential direction. Two possible layouts that fulfil this requirement are shown in Fig. 3. Based on an unfolded view of the mover, the PM pole sizes in axial and circumferential direction can be identified and are denoted by τ_z and τ_φ, respectively. Subsequently, the proposed layouts are referred to as DM and SM, for the arrangements featuring diamond-shaped PMs (see Fig. 3(a)) and square-shaped PMs (see Fig. 3(b)), respectively.

Figure 4 shows the radial component of the PM flux density B_r at the inner and outer side of the mover. The alternation of the PM poles in the axial and circumferential direction is clearly visible for the CM (see Fig. 4(a)). For the DM and SM, the PM pole alternation is interrupted compared to the CM. Nevertheless, a higher magnitude of the PM flux density is possible for the DM and SM for the given mover thickness because of thicker PMs. While the magnitude of B_r for the CM is $\approx 0.38\,\mathrm{T}$, $\hat{B}_r \approx 0.52\,\mathrm{T}$ is reached for the DM and SM.

The unfolded version of the PM arrangement shown in Fig. 3 is used in planar actuator systems. For example, a synchronous PM planar motor with a similar PM arrangement is shown in [9]. A magnetically levitated moving-magnet planar actuator with single layer windings in the stator is proposed in [10]. A planar actuator with multilayer windings in the stator and a PM arrangement in the mover that is similar to the unfolded DM (see Fig. 3(b)) is analysed and optimized in [11].

A LiRA with a PM arrangement as shown in Fig. 3(b) and a single stator is proposed in [12]. The stator of this LiRA is slotted with double layer windings, i.e. linear and rotary windings, that are radially displaced. The manufacturing effort of such a stator is high as the stator core is slotted both in circumferential and axial direction. Another LiRA, again with PM arrangements as shown in Fig. 3, is proposed in [13]. Linear and rotary actuation in this LiRA are achieved by two separated stators, which are dislocated circumferentially. This results in several drawbacks of the system, such as the requirement for a back iron in the mover and the existence of a radial magnetic pull originating from the asymmetrical LiRA geometry in the circumferential direction. In the proposed DS LiRA, no radial magnetic pull exists, since the radial dislocation of the stators results in a symmetrical geometry.

III. BASIC CHARACTERISTICS OF THE CONVENTIONAL AND PROPOSED DOUBLE STATOR ACTUATORS

In this section, a comparative analysis of the DS LiRA with CM and the proposed DS LiRAs with a DM and SM is provided. The back iron in the CM amounts for about half of the mover thickness (see the proposed designs in [14]). If the mover contains only PMs, $r_m = r_{pm,in} + r_{pm,out}$ holds. In order to obtain a fair comparison, only PM material is assumed in the movers. Therefore, the back iron of the CM is replaced by PM material and the mover thickness is shared equally between the inner and outer PMs, $r_{pm,in} = r_{pm,out}$ (see Fig. 5), resulting in a *theoretical idealised* CM (iCM). In the DM and the SM, no mechanical support is assumed,
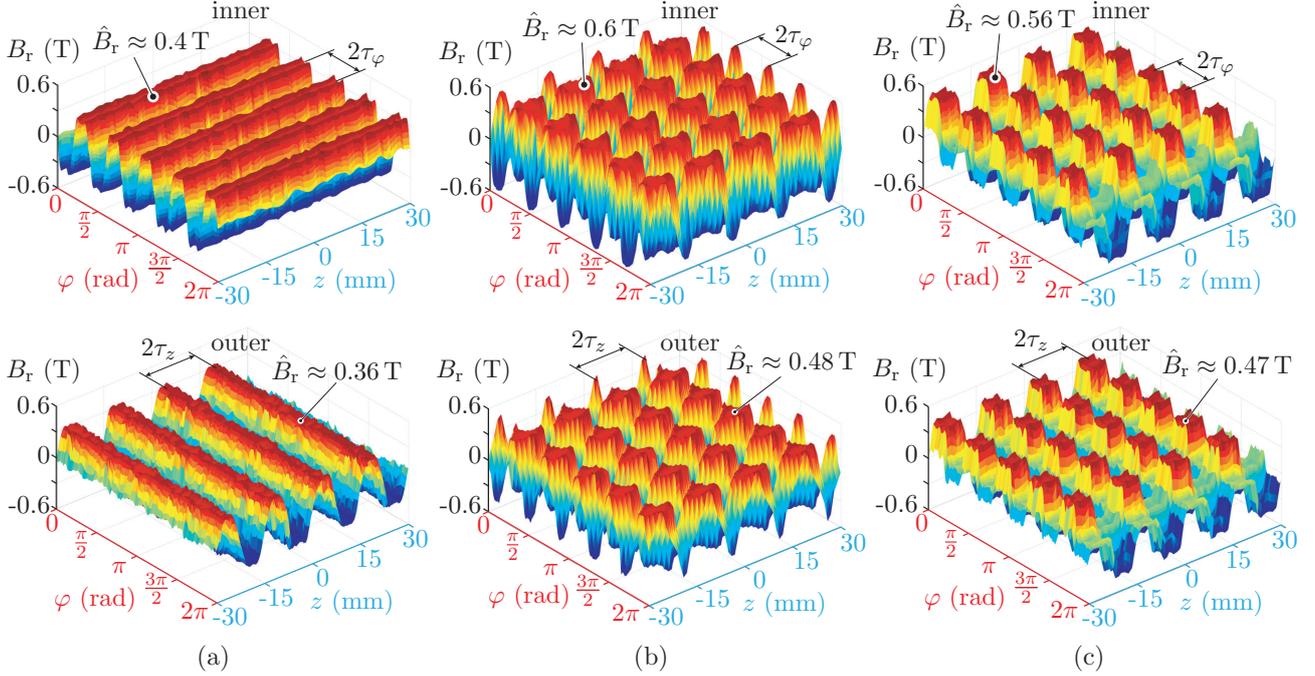
Fig. 4: FEM simulation of the radial flux density component B_r at the inner and outer side of the mover: (a) CM, (b) DM, and (c) SM. The inner and outer radii for all movers are $11.5\,\text{mm}$ and $15.5\,\text{mm}$, respectively. The radial positions for which B_r is shown are $11.15\,\text{mm}$ for the inner side and $15.85\,\text{mm}$ for the outer side. The rest of the parameters are given in Tab. I. Pole pair sizes in axial and circumferential directions are denoted by τ_z and τ_φ, respectively.
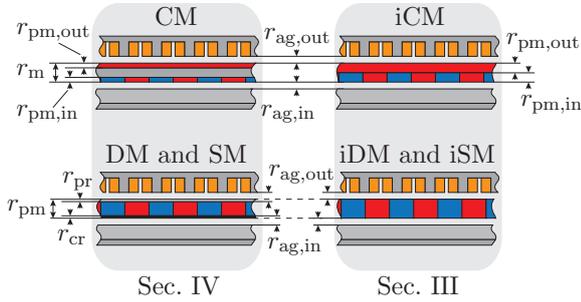
Fig. 5: Summary of the analysis scenarios. Initial analysis is conducted in Sec. III, in which the movers are solely made of PM material. Therefore, for CM there is no back-iron and for DM and SM there is no any mechanical support. In Sec. IV, DS LiRAs with physically manufacturable movers are further analysed and compared. Inner and outer magnetic air gaps are denoted as $r_{ag,in}$ and $r_{ag,out}$, respectively. Inner and outer mechanical air gaps are equal to $r_{ag,in} - r_{cr}$ and $r_{ag,out} - r_{pr}$, respectively, where r_{cr} and r_{pr} are carbon rod and PM protection thicknesses (see Sec. IV).

TABLE II: Parameters of the DS LiRAs for which the performance is shown in Fig. 6.

Parameter (Symbol)	Values		
PM remanent flux density	1.3 T		
Iron relative permeability	500		
PM mass density	$7550\,\text{kg}\,\text{m}^{-3}$		
Iron mass density	$7870\,\text{kg}\,\text{m}^{-3}$		
Stator length (L)	60 mm		
Outer stator diameter (D)	50 mm		
Number of poles (N_φ)	10		
Number of poles (N_z)	8		
Pole size (τ_φ)	36°		
Pole size (τ_z)	7.5 mm		
Inner and outer air gaps	0.7 mm		
Stator back iron thickness	2 mm		
	iCM	**iDM**	**iSM**
Inner PM thickness ($r_{pm,in}$)	1-2 mm	-	-
Outer PM thickness ($r_{pm,out}$)	1-2 mm	-	-
Mover back iron (r_{iron})	0	-	-
PM thickness (r_{pm})	-	1-4 mm	1-4 mm
Mover thickness (r_m)	2-4 mm	1-4 mm	1-4 mm

which also results in *theoretical* idealised DM and SM (iDM and iSM). It should be noted that such movers cannot be manufactured and therefore are used only for the first step comparative purposes in this section.

The comparison is carried out considering rare-earth PMs. The parameters of the compared LiRAs are provided in Tab. II. The available space in radial direction is shared equally between the inner (rotary) and outer (linear) actuator windings. The force and torque of each analysed LiRA are determined using magnetostatic finite element method (FEM) models. The electrical loading is chosen such that 15 W of copper losses are dissipated in each of the actuators. This assumed value for the electrical loading stems from the simplified lumped-parameter thermal model that was established for tubular actuators of similar size in [14]. While the actual admissible electrical loading depends on the application and available cooling of the LiRA, the assumed constant electric loading provides a good basis for relative comparison.

A comparison of the axial force and acceleration is shown
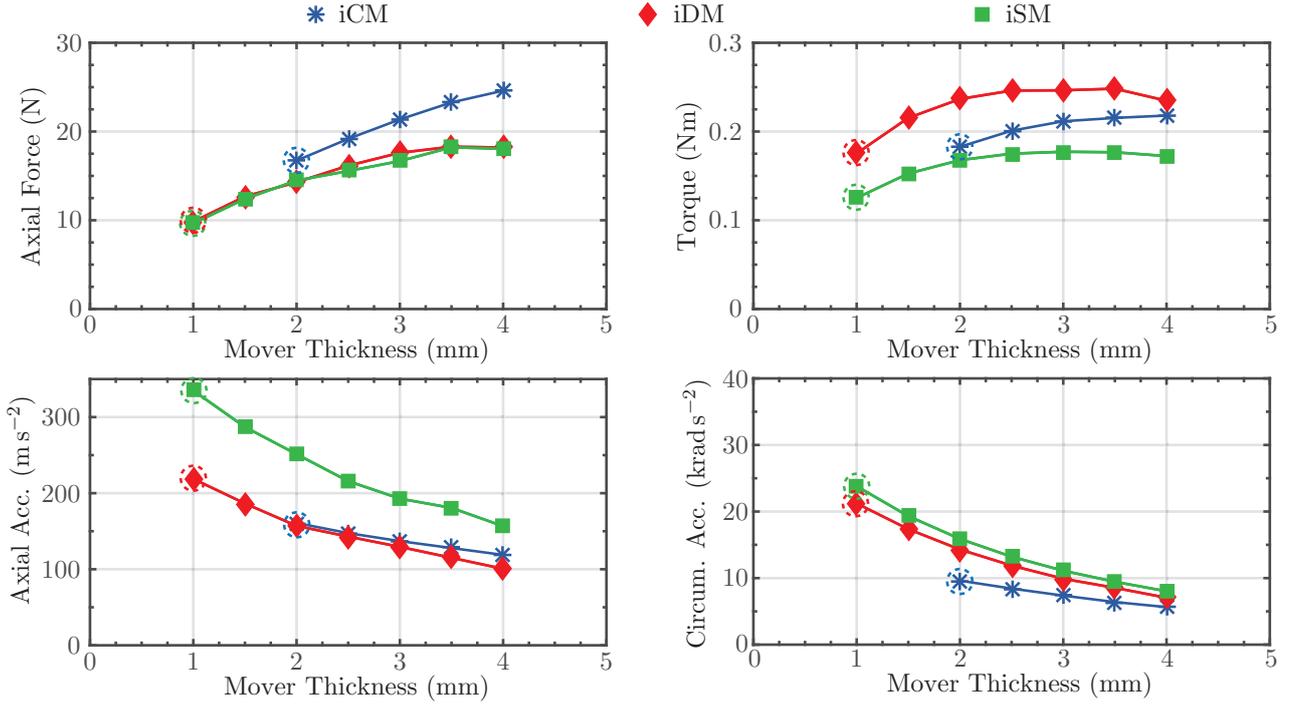
Fig. 6: Comparison of the DS LiRAs with three different mover layouts: iCM (blue), iDM (red) and iSM (green). Axial and circumferential accelerations are calculated using only the mass and moment of inertia of the mover. Material and geometry properties are given in Tab. II. The results are obtained using FEM models in which winding copper losses are fixed to 15 W for all designs. Circled simulation points are relatively compared in Fig. 7.

in Fig. 6 on the left hand side, while a comparison of the torque and circumferential accelerations is shown in Fig. 6 on the right hand side. The analysis has been carried out for different mover thicknesses, where the FEM simulation points are marked by blue asterisks (✳) for the DS LiRA with iCM, red rhomboids (◆) for the DS LiRA with iDM and green squares (■) for the DS LiRA with iSM. The minimum PM thickness has been set to 1 mm, which results in a minimum mover thickness of the iCM of 2 mm, since it has two sets of PMs displaced radially. Contrarily, the minimum thickness of the iDM and iSM is 1 mm.

Even though the axial force of the DS LiRA with iCM is the highest, the iSM reaches the highest axial acceleration. This is due to the PM volume in the iSM being almost cut in half compared to the iCM or iDM. A similar trend can be observed for the circumferential LiRA properties. The circumferential acceleration of the LiRAs with the iDM and iSM is similar, while the iDM features a higher torque.

A relative comparison of the achievable torque, force, and accelerations, for the same copper losses in the actuator windings, is shown in Fig. 7. Compared to the iCM, the proposed mover layouts (see Fig. 3) can achieve higher axial and circumferential accelerations for the same amount of copper losses.

IV. Manufacturing of the Proposed Double Stator Actuator

Manufacturing constraints and their influence on the design and the performance of the actuator are studied in detail in this section. The proposed mover concepts were shown in Fig. 3
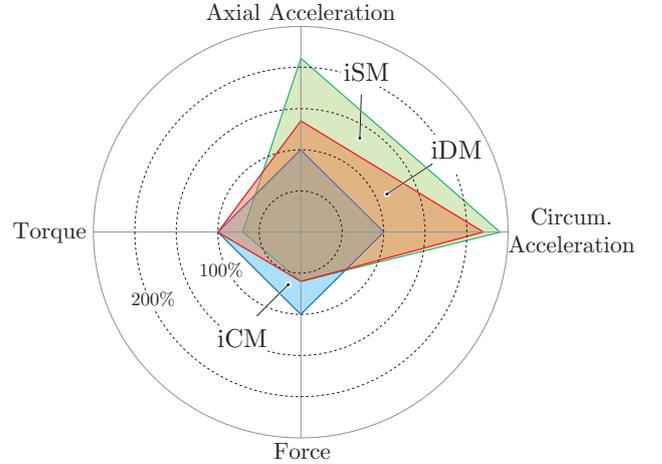
Fig. 7: Relative comparison of the circled designs from Fig. 6 with a PM thickness of 1 mm. The mover thickness is 2 mm for the iCM and 1 mm for the iDM and iSM. Compared designs are circled in Fig. 6.

without any mechanical support. The suggested manufacturing steps for the DM are outlined in Fig. 8. The complete mover consists of three parts: a carbon rod, a 3D-printed fixture for the PMs, and the PMs. The ease of manufacturing of such an arrangement, compared to the CM with two sets of PMs, has several advantages. The PMs for the CM have to be fixed to both sides of the back iron (see Fig. 2(b)), which

is a challenging task considering the forces between the PMs. Moreover, the PMs are prone to breaking due to their small thickness to length ratio

$$\frac{r_{\text{pm}}}{L_{\text{m}}} \approx \frac{1}{90}, \tag{1}$$

when optimized for high dynamics [14], see Fig. 2(b). Contrarily, all PMs feature the same shape (e.g. north and south poles for the DM shown in Fig. 8) in the proposed manufacturing scenario, which simplifies fabrication. The PM pieces are mounted from only one side of the mover and the risk of breaking is low, as the thickness to length ratio is higher. The proposed mechanical support for the SM is conceptually the same, with the 3D-printed fixture (see Fig. 8) having a shape that suits the respective PM arrangement (see Fig. 3(b)).
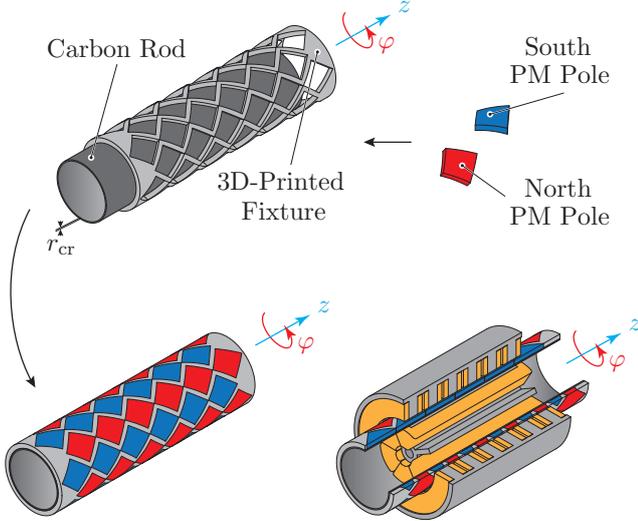
Fig. 8: Manufacturing concept for the proposed double stator actuator. The thickness of the carbon rod is $r_{\text{cr}} = 0.5\,\text{mm}$.

Another important manufacturing aspect of the DS LiRA is the radial support of the mover. The conventional approach is to use mechanical bearings or air bearings. Such bearings require an additional mechanical assembly, which increases the mass and moment of inertia of the mover. To overcome this disadvantage, the proposed concept is planned to employ magnetic bearings (MBs) [15] in the final realization.

A. Performance Comparison

Introduction of the mechanical support for the DM (see Fig. 8) and SM influences the DS LiRA design and performance, i.e. it increases the size of the mover and the magnetic air gap (see Fig. 5). The related effects on the performance are shown in Fig. 9. An electrical loading resulting in $15\,\text{W}$ of copper losses is chosen, which is identical to that used above. The geometrical parameters, physical properties, and absolute values of the performance with included manufacturing limitations are given in Tab. III. In order to consider a lightweight carbon rod with a wall thickness of $r_{\text{cr}} = 0.5\,\text{mm}$ for the mechanical support of the proposed DM and SM, the inner magnetic air gap is enlarged to $1.2\,\text{mm}$. The outer air gap is also enlarged to $1.2\,\text{mm}$, providing increased space for additional mechanical protection of the PMs. These manufacturing constraints degrade the performance of the proposed DS LiRAs, which is seen from the comparison of Fig. 7 and
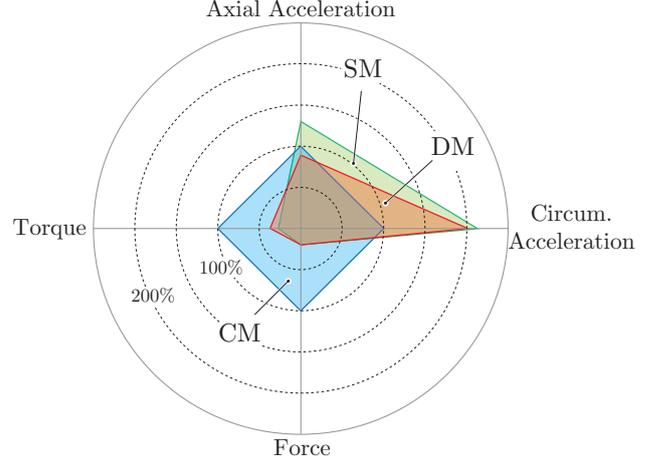
Fig. 9: Relative comparison of the designs from Fig. 7 with manufacturing limitations being considered.

TABLE III: DS LiRAs with included manufacturing constraints.

Parameter	Values		
Number of poles in RA	10		
Number of poles in LA	8		
Number of slots in RA	6		
Number of poles in LA	6		
Geometrical parameters	**CM**	**DM**	**SM**
Inner PM thickness ($r_{\text{pm,in}}$)	1 mm	-	-
Outer PM thickness ($r_{\text{pm,out}}$)	1 mm	-	-
Mover back iron (r_{iron})	2 mm	-	-
PM thickness (r_{pm})	-	1 mm	1 mm
Carbon rod thickness (r_{cr})	-	0.5 mm	0.5 mm
PM mechanical protection (r_{pr})	-	0.5 mm	0.5 mm
Mover thickness (r_{m})	4 mm	1 mm	1 mm
Magnetic air gaps	0.7 mm	1.2 mm	1.2 mm
Mechanical air gaps	0.7 mm	0.7 mm	0.7 mm
Physical properties (Unit)			
Mover mass (g)	240	52	36
Mover MoM ($\times 10^{-6}\text{kg m}^2$)	51.5	9.35	6.54
Performance (Unit)			
Axial force (N)	35.9	7.1	7.0
Torque (N m)	0.3	0.11	0.081
Axial acc. (m s^{-2})	150	134	194
Circumferential acc. (rad s^{-2})	5825	11 764	12 393

Fig. 9. The accelerations for the DS LiRA with DM and SM are calculated including the mass and moment of inertia of the carbon rod and 3D-printed fixture. Even with the included manufacturing constraints, the proposed DS LiRAs achieve higher accelerations than a DS LiRA with CM.

B. Cogging Torque and Force

Due to the interaction of the mover PMs with the inner and outer stator iron, a cogging torque T_{cog} and a cogging force F_{cog} act on the mover. The amplitude of the cogging torque/force can be estimated by [16]

$$\{T_{\text{cog}}, F_{\text{cog}}\} \sim \phi^2 \frac{dR}{d\{\varphi, z\}}, \tag{2}$$

where ϕ denotes the PM flux crossing the air gap and R is the total reluctance through which the flux passes. The waveform of the cogging torque/force can be described by means of a

Fourier series expansion [17], [18]. The fundamental period of the cogging torque/force can be determined as [16], [19]

$$\tau_{\text{cog}}^{\{\text{T,F}\}} = \frac{\{360°, L\}}{\text{LCM}(N_\text{s}, N_\text{p})}, \quad (3)$$

where L is the stator length of the linear actuator, N_s is the total number of slots in the stator (either linear or rotary), N_p is the number of poles (for the linear actuator N_p is the number of poles covered by the stator, while in the rotary actuator N_p is the total number of poles), and LCM() denotes the least common multiple function. The fundamental cogging torque period for the rotary actuator is

$$\tau_{\text{cog}}^{\text{T}} = \frac{360°}{\text{LCM}(6, 10)} = 12°, \quad (4)$$

while the period of the fundamental component of the cogging force for the linear actuator is

$$\tau_{\text{cog}}^{\text{F}} = \frac{60\,\text{mm}}{\text{LCM}(6, 8)} = 2.5\,\text{mm}. \quad (5)$$

Cogging torque waveforms of the DS LiRA designs from Tab. III are shown in Fig. 10. The period of the fundamental
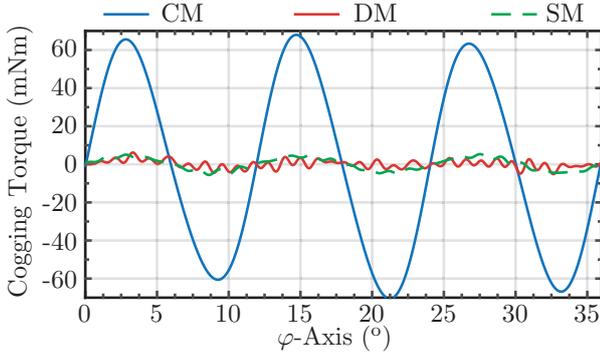
Fig. 10: Cogging torque of the DS LiRA designs given in Tab. III.

component of the cogging torque is estimated by curve fitting of the waveforms. As a cogging torque (or force) is undesired (especially in high-precision positioning systems), it is usually compensated for by feedforward control of a current reference that depends on the circumferential and axial position φ and z, respectively. The current component that compensates for the cogging torque increases the copper losses in the rotary actuator windings of the DS LiRA with CM by about $0.4\,\text{W}$, which is very low due to quadratic dependence of the losses and electromagnetic torque. Hence, the increase of copper losses in the DM and SM LiRAs for this compensation is negligible.

Cogging force waveforms of the DS LiRA designs given in Tab. III are shown in Fig. 11 for an axial stroke of the mover from $-7.5\,\text{mm}$ to $7.5\,\text{mm}$. The period of the fundamental component of the cogging force is estimated by curve fitting of the waveforms from Fig. 11. This obtained value agrees with $\tau_{\text{cog}}^{\text{F}}$ calculated in (5). Compensation of the cogging force waveform by a feedforward current increases copper losses of the DS LiRA with CM by $0.5\,\text{W}$. Again, the increase of copper losses for this compensation in the DM and SM LiRA is negligible.
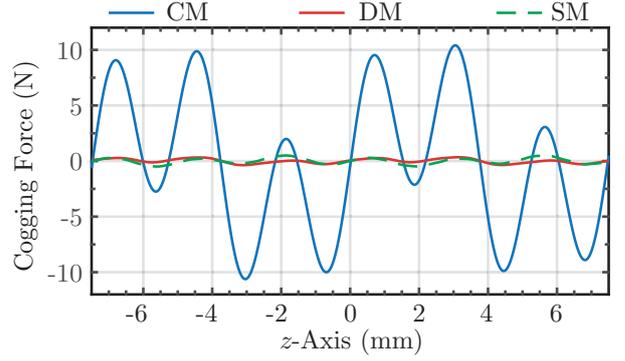
Fig. 11: Cogging force of the DS LiRA designs given in Tab. III.
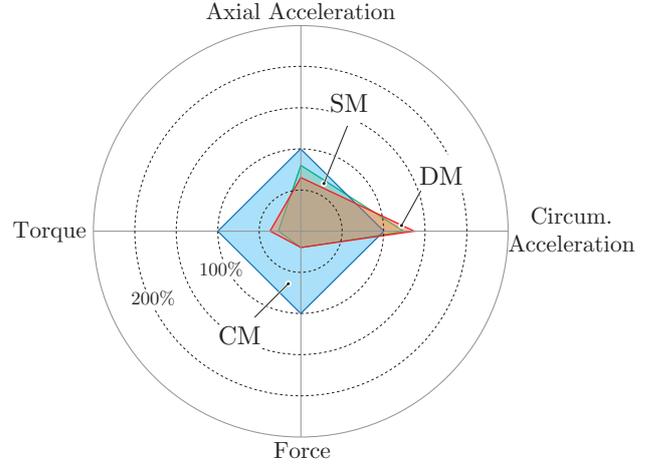
Fig. 12: Relative comparison of the performance with a load.

C. Influence of Mechanical Load

In manufacturing applications, a DS LiRA can be used to pick and place different objects, e.g. electronic components that are placed on a printed circuit board. The mass and inertia of such components are negligibly low. However, in order to carry these components, a nozzle needs to be mounted to the end of the mover. Considering the dimensions of the mover, a nozzle with $m_{\text{load}} = 30\,\text{g}$ and $I_{\text{load}} = 6 \times 10^{-6}\,\text{kg}\,\text{m}^2$ is assumed to be attached to the mover. Consequently, the DS LiRA designs from Tab. III have a modified mass and moment of inertia of the movers, resulting in the updated performance characteristics provided in Tab. IV. The relative reduction of the performance is shown in Fig. 12. Therefore, special care should be taken when designing a DS LiRA with a DM or SM, as its performance (acceleration) strongly depends on the additional mechanical load. The later depends on the application of the DS LiRA, for which a further application-specific optimization is possible.

D. Summary of the Conducted Comparison

Double stator LiRAs with CM, DM and SM are compared in this section in terms of actuation properties (achievable torque and force), dynamics (circumferential and axial accelerations), cogging torque and cogging force. DS LiRA with CM achieves higher torque and force, which in some applications are not

TABLE IV: Performance of DS LiRAs with a mechanical load attached to the mover.

Parameter	Values		
Physical properties (Unit)	**CM**	**DM**	**SM**
Mover mass (g)	270	82	66
Mover MoM ($\times 10^{-6}$ kg m^2)	57.5	15.35	12.54
Performance (Unit)			
Axial force (N)	35.9	7.1	7.0
Torque (N m)	0.3	0.11	0.081
Axial acc. (m s^{-2})	133	86.6	106.1
Circumferential acc. (rad s^{-2})	5217	7166	6459

Planar SM

PMs 3D Printed Fixture

Planar Stator

Winding

Planar DS LiRA

Upper Stator Planar SM

25cm

25cm
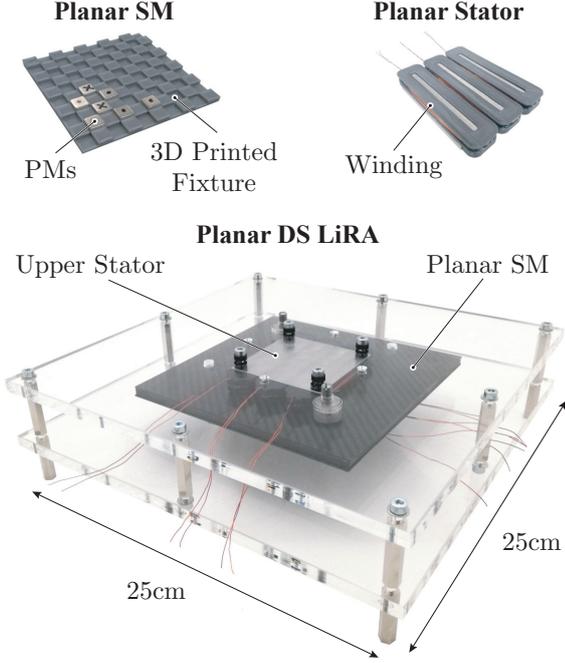
Fig. 13: Simplified planar hardware setup. Not all PMs are mounted in the photo of the planar SM.

needed (e.g. high speed pick-and-place packaging robots) as throughput is determined by accelerations. Proposed DS LiRAs with DM or SM have doubled circumferential acceleration and about 30 % higher axial acceleration in the case there is no load at the mover, see Fig. 9. The additional load can deteriorate dynamics, which is shown in Fig. 12 where additional load with $m_{\text{load}} = 30$ g and $I_{\text{load}} = 6 \times 10^{-6}$ kg m^2 is assumed. Nevertheless, it should be kept in mind that manufacturing of DS LiRAs with DM and SM is simpler. Cogging torque and force of the proposed DS LiRAs with DM and SM are much lower, see Fig. 10 and Fig. 11, which is important aspect as the they cause disturbance in positioning systems.

V. SIMPLIFIED PLANAR HARDWARE SETUP

In order to verify the FEM models used in the analysis, a simplified planar actuator is implemented. The hardware setup of the actuator is shown in Fig. 13. It consists of a planar mover and two planar stators, which are placed above and below the mover. Each of the stators features three concentrated coils with 100 turns of insulated copper wire
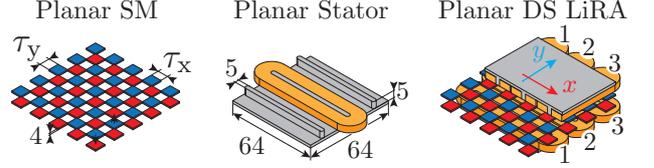
Fig. 14: Geometry and the coordinate system of the simplified planar hardware setup. All dimensions are in mm. The upper and lower air gaps are 2.2 mm. Pole sizes are $\tau_x = \tau_y = 8$ mm.

TABLE V: Comparison of simulated and measured results for the flux linkage.

Lower Stator			
Flux linkage	FEM simulation		3.4 mWb
Flux linkage	Measurement		3.3 mWb

with a diameter of 0.4 mm. The implemented mover resembles the SM type analysed in this paper. During the manufacturing procedure of the mover, the PMs are initially arranged in a 3D printed fixture (see Fig. 13), before 1 mm thick carbon fiber plates are glued from both sides for mechanical stability. The dimensions of the stator and the mover geometry are provided in Fig. 14.

The comparison of the FEM simulation results with measurements is carried out for the flux linkage. The measurement results for the flux linkage are obtained by integrating the induced back-emf in the windings of the lower and upper stators. To induce the back-emf, the mover is driven in the y-axis direction (see Fig. 14 for the orientation of the coordinate system).

Further, the flux linkage is studied for different mover positions in the y-axis by using an FEM model of the planar setup. In Fig. 15, the flux linkage waveforms are shown for a single winding turn of the lower and upper stator coils. The flux linkage for the turns in the lower stator is $\approx 34\,\mu$Wb. This value is multiplied by the number of turns of the manufactured coils (100) and compared to the measured flux linkage in Tab. V. The results show a good agreement of the measurement and FEM simulation results, which verifies the correctness of the employed FEM models.

The waveform of the flux linkage in the lower stator can be modeled as

$$\psi_{\text{L}}(y(t)) = N \hat{\Psi}_{\text{L,y}} \cos\left(\frac{\pi}{\tau_y} y(t)\right), \quad (6)$$

where N represents the number of turns in the coil, $\hat{\Psi}_{\text{L,y}} = 34\,\mu$Wb from Fig. 15, and $\tau_y = 8$ mm is the pole size in the y direction. The flux linkage in the upper stator due to the same movement in the y direction is modeled as

$$\psi_{\text{U}}(y(t)) = N \hat{\Psi}_{\text{U,y}} \cos\left(\frac{\pi}{\tau_y} y(t)\right) + \psi_{\text{U,offset}}(x(t)), \quad (7)$$

where $\hat{\Psi}_{\text{U,y}} = 2.75\,\mu$Wb from Fig. 15 and $\psi_{\text{U,offset}}(x(t))$ is the offset that depends on the x position of the mover. $\hat{\Psi}_{\text{U,y}}$ represents an undesired coupling, since ideally no change of the flux linkage in the upper stator is expected for a movement in the y direction. The ratio of the induced back-emf amplitudes in the upper and lower stator windings due to a movement in the y direction is $E_{\text{U}}/E_{\text{L}} = \hat{\Psi}_{\text{U,y}}/\hat{\Psi}_{\text{L,y}} \approx$
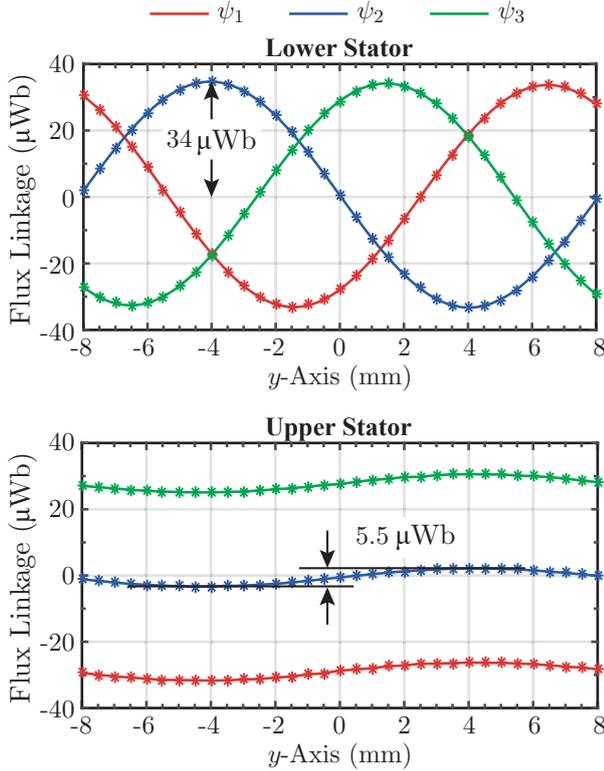
Fig. 15: FEM simulation results for the flux linkage per turn of the lower and upper stators of the planar setup shown in Fig. 14. Flux linkages ψ_1, ψ_2 and ψ_3 are flux linkages of the coils 1, 2 and 3 of the lower and upper stator, respectively. Asterisks represent FEM simulation points. The coil numbers are denoted in Fig. 14 (right).

8.1 %. Therefore, for the planar actuator shown in Fig. 14, the undesired back-emf is about 8.1 % of the expected back-emf. Coupling effects between the stators in the LiRA, with a DM or SM, will be studied in future work.

VI. CONCLUSIONS

State-of-the-art double stator (DS) linear-rotary actuators (LiRAs) are mainly used in high force/torque applications, such as tooling machines. Their usage in highly dynamic applications is limited by the bulky mover design, referred here as <u>c</u>onventional <u>m</u>over (CM). CMs employ two sets of permanent magnets (PMs) and a back iron. In order to increase the dynamics of the DS LiRA, two different ironless mover concepts with a single set of PMs (DM and SM) are proposed in this paper. Moreover, manufacturing steps for the proposed mover layouts are provided. After accounting for manufacturing constraints, an axial acceleration of the proposed DS LiRA with the SM is around 30 % higher than that of a DS LiRA with the CM, while the circumferential acceleration nearly doubles. Additionally, the cogging torque and the cogging force of the proposed DS LiRAs are negligible compared to those of the DS LiRA with the CM. Manufacturing of the proposed movers (DM and SM) is simpler. On the other hand, due to lower torque and force of the DS LiRAs with DM and SM, accelerations decrease faster when additional load is attached to the mover than that of the DS LiRA with the CM.

The advantage of a CM having two sets of magnets is that the mover can be optimised either for high circumferential or axial acceleration, which is not possible with proposed DM and SM as they feature a single set of magnets.

REFERENCES

[1] A. Turner, K. Ramsay, R. Clark, and D. Howe, "Direct-Drive Rotary-Linear Electromechanical Actuation System for Control of Gearshifts in Automated Transmissions," in *IEEE Vehicle Power and Propulsion Conference*, 2007, pp. 267–272.

[2] J. Pan, Y. Zou, and N. C. Cheung, "Performance Analysis and Decoupling Control of an Integrated Rotary-Linear Machine with Coupled Magnetic Paths," *IEEE Transactions on Magnetics*, vol. 50, no. 2, pp. 761–764, 2014.

[3] S. Tanaka, T. Shimono, and Y. Fujimoto, "Optimal Design of Length Factor for Cross-Coupled 2-DOF Motor with Halbach Magnet Array," in *IEEE International Conference on Mechatronics (ICM)*, 2015, pp. 529–534.

[4] T. Overboom, J. Jansen, E. Lomonova, and F. Tacken, "Design and Optimization of a Rotary Actuator for a Two Degree-of-Freedom $z - \varphi$ Module," in *IEEE International Electric Machines and Drives Conference (IEMDC)*, 2009, pp. 1043–1050.

[5] T. J. Teo, H. Zhu, S.-L. Chen, G. Yang, and C. K. Pang, "Principle and Modeling of a Novel Moving Coil Linear-Rotary Electromagnetic Actuator," *IEEE Transactions on Industrial Electronics*, vol. 63, no. 11, pp. 6930–6940, 2016.

[6] K. Meessen, J. Paulides, and E. Lomonova, "Analysis and Design Considerations of a 2-DoF Rotary-Linear Actuator," in *IEEE International Electric Machines & Drives Conference (IEMDC)*, 2011, pp. 336–341.

[7] L. Xu, M. Lin, X. Fu, and N. Li, "Design and Analysis of a Double-Stator Linear-Rotary Permanent-Magnet Motor," *IEEE Transactions on Applied Superconductivity*, vol. 26, no. 4, pp. 1–4, 2016.

[8] S. M. Jang, S. H. Lee, H. W. Cho, and S. K. Cho, "Design and Analysis of Helical Motion Permanent Magnet Motor with Cylindrical Halbach Array," *IEEE Transactions on Magnetics*, vol. 39, no. 5, pp. 3007–3009, 2003.

[9] H.-S. Cho and H.-K. Jung, "Analysis and Design of Synchronous Permanent-Magnet Planar Motors," *IEEE Transactions on Energy Conversion*, vol. 17, no. 4, pp. 492–499, 2002.

[10] J. Jansen, C. Van Lierop, E. A. Lomonova, and A. J. Vandenput, "Magnetically Levitated Planar Actuator With Moving Magnets," *IEEE Transactions on Industry Applications*, vol. 44, no. 4, pp. 1108–1115, 2008.

[11] L. Guo, H. Zhang, M. Galea, J. Li, and C. Gerada, "Multiobjective Optimization of a Magnetically Levitated Planar Motor With Multilayer Windings," *IEEE Transactions on Industrial Electronics*, vol. 63, no. 6, pp. 3522–3532, 2016.

[12] L. Chen and W. Hofmann, "Design of One Rotary-Linear Permanent Magnet Motor with Two Independently Energized Three Phase Windings," in *Proc. of* 7$^\text{th}$ *International Conference on Power Electronics and Drive Systems (PEDS)*, 2007, pp. 1372–1376.

[13] A. Chitayat and M. Faizullabhoy, "System and Method to Control a Rotary-Linear Actuator," May 2007, US Patent 7,218,017.

[14] S. Mirić, A. Tüysüz, and J. W. Kolar, "Comparative Evaluation of Linear-Rotary Actuator Topologies for Highly Dynamic Applications," in *Proc. of IEEE International Electric Machines and Drives Conference (IEMDC)*, 2017, pp. 1–7.

[15] H. Bleuler, M. Cole, P. Keogh, R. Larsonneur, E. Maslen, Y. Okada, G. Schweitzer, A. Traxler *et al.*, *Magnetic Bearings: Theory, Design, and Application to Rotating Machinery*. Springer Science & Business Media, 2009.

[16] D. C. Hanselman, *Brushless Permanent Magnet Motor Design*. The Writers' Collective, 2003.

[17] L. Zhu, S. Jiang, Z. Zhu, and C. Chan, "Analytical Methods for Minimizing Cogging Torque in Permanent-Magnet Machines," *IEEE Transactions on Magnetics*, vol. 45, no. 4, pp. 2023–2031, 2009.

[18] P. Hor, Z. Zhu, D. Howe, and J. Rees-Jones, "Minimization of Cogging Force in a Linear Permanent Magnet Motor," *IEEE Transactions on Magnetics*, vol. 34, no. 5, pp. 3544–3547, 1998.

[19] N. Bianchi, S. Bolognani, and A. Cappello, "Reduction of Cogging Force in PM Linear Motors by Pole-Shifting," *IEE Proceedings-Electric Power Applications*, vol. 152, no. 3, pp. 703–709, 2005.